

Visual Analysis of Cerebral Perfusion Data —Four Interactive Approaches and a Comparison—

Steffen Oeltze and Bernhard Preim
Dept. of Simulation and Graphics
Univ. of Magdeburg, Germany
stoeltze{preim}@isg.cs.uni-magdeburg.de

Jarle Rørvik
Dept. of Surgical Sciences & Dept. of Radiology
Univ. of Bergen & Haukeland Univ. Hospital, Norway
jarle.rorvik@helse-bergen.no

Helwig Hauser
Dept. of Informatics
Univ. of Bergen, Norway
Helwig.Hauser@UiB.no

Arvid Lundervold
Dept. of Biomedicine
Univ. of Bergen, Norway
arvid.lundervold@biomed.uib.no

Abstract

Cerebral perfusion data are acquired to characterize the regional blood supply of brain tissue. One of their major diagnostic applications is ischemic stroke assessment. We present a comparison of four interactive approaches to analyzing cerebral perfusion data from ischemic stroke patients which are based on (1) concentration-time curves (CTC) derived from the original data, (2) parameters describing the CTC shape, (3) enhancement trends computed in a statistical analysis, and (4) semi-quantitative perfusion parameters derived via parametric modelling and deconvolution. The comparison is carried out with regard to the involved data pre-processing, the complexity of the interactive analysis and the resulting tissue selections. It is supported by a visual analysis framework that integrates the different approaches. The rich information content in time-dependent 3D perfusion data is both an opportunity for improved diagnosis and a challenge how to optimize the assessment of such rich data. With our comparison we contribute to a discussion between data-near and model-near assessment strategies and their respective opportunities.

1. Introduction

In the U.S., stroke ranks number three among all causes of death, when considered separately from other cardiovascular diseases [5]. Of all strokes, 87% are ischemic. In the event of an ischemic stroke, an artery supplying the brain with blood is blocked. This leads to a death of brain cells due to a sustained undersupply of oxygen and nutrients.

Primarily, Computed Tomography (CT) and Magnetic Resonance Imaging (MRI) are used to assess a stroke in clinical routine. Compared to CT, MRI offers a better contrast-resolution and options to image the brain with multiparametric techniques in all anatomic orientations facilitating a better detection and localization of infarctions. Hence,

we focus on MR perfusion but our concepts can be readily transferred to CT perfusion.

The brain tissue affected by an ischemic stroke can be classified into irreversibly damaged tissue (core) and *tissue-at-risk* (penumbra). The penumbra may be salvaged by an intervention removing the blood clot within a time window of ≈ 6 hours after symptom onset [14]. It has been reported as a predictor for the final infarction size [15].

In cerebral perfusion imaging, the spatio-temporal distribution of a contrast agent (CA) is recorded to assess blood volume and flow. For each voxel, a time-intensity curve (TIC) characterizes the CA enhancement. Changes in signal intensity are often converted to changes in CA concentration resulting in concentration-time curves (CTC) [12]. Perfusion parameters describing the curve shape during the CA's first pass through the brain tissue are derived voxel-wise (Fig. 3). The computation of quantitative parameters from MR perfusion is ongoing research [18]. No absolute thresholds can yet be reliably computed for identifying ischemic tissue. Instead, new approaches classify tissue by identifying common properties of signal dynamics [4], [6].

We provide an interactive alternative to these approaches spearheaded by a feature definition component. The interactivity accounts for the uncertainty involved in the classification process. The user also gains a better insight into the data by interactively changing the feature definition and observing the updated selection result. We base the feature definition on four different inputs: (1) CTCs, (2) parameters describing the CTC shape, (3) enhancement trends computed in a statistical analysis, and (4) semi-quantitative perfusion parameters derived via parametric modelling and deconvolution. We compare the approaches regarding the involved data pre-processing, the complexity of the interactive analysis and the resulting tissue selections. Our visual analysis approach primarily addresses researchers seeking for a better understanding of which perfusion parameters are crucial for specific diagnostic tasks, how they are related and how imaging parameters influence their expressiveness.

2. Related Work

Our visual analysis concept is closely related to systems for analyzing and exploring medical multi-field data such as [1]. In particular, we also employ the concept of integrating a 3D visualization with multiple statistical representations, connected by brushing facilities. Our concept has been presented in the context of perfusion data from different application areas in [9] and is here adapted to and investigated particularly for cerebral perfusion. In the following, we will briefly review existing approaches to the visual analysis of perfusion data. See [11] for a detailed survey.

Coto et al. [2] presented several investigation tools (e.g., scatterplot and volume rendering) for the classification and visualization of Dynamic contrast-enhanced MRI mammography data. Their approach combines brushing and linking interaction on enhancement scatterplots with effective 3D visualization of the selected suspicious areas. Mlejnek et al. [7] proposed the *Application Profile Flag*, an intuitive tool for probing and annotating of temporal data. It enables the visualization of spatial or temporal curves closely connected to the rendering of the anatomic structure of the data without removing any parts thereof.

In our previous work, statistical analysis techniques and advanced scientific and information visualization techniques have been combined in order to efficiently explore the space of perfusion parameters [9]. In particular, a correlation analysis is carried out followed by a Principal Component Analysis in order to detect major trends. Inspired by the work of Doleisch et al. [3], the trends as well as the original perfusion parameters are displayed in 2D-histograms and scatterplots and are used for brushing of relevant subsets of the data. This overall strategy turned out to be useful to discriminate different tissues in cerebral perfusion, breast tumor perfusion and myocardial perfusion data. The combination of analysis techniques with linking and brushing has been extended with a dense visualization of TICs for all voxels of a perfusion data set [8].

3 Method

This section starts with a description of the image data our work is based on. Next, the crucial pre-processing steps are described. Finally, four interactive approaches to investigating cerebral perfusion data are presented.

3.1 Image Data

We tested our visual analysis approaches based on two perfusion studies from two patients, who both suffered from an acute ischemic stroke. In both cases, the parietal lobe in either of the two hemispheres was affected by a thrombosis of the middle cerebral artery. The second study consists of three scans acquired ≈ 2 hours after symptom onset, ≈ 4 hours later, after thrombolytical treatment (≈ 3 hours after symptom onset), and the next day. Typical sequence parameters for the first DSC-MRI perfusion study PS and the

follow-up study PS_{fup} (in brackets if different from PS) are: Gradient echo planar imaging (EPI) with TR = 2000ms, TE = 53.7ms (60.7ms), matrix = 128×128 , slice thickness = 6mm (5mm), slice gap = 1.02mm (1.5mm), in-plane resolution = $1.7 \times 1.7 \text{mm}^2$ ($1.9 \times 1.9 \text{mm}^2$), number of slices = 12 (15), number of acquisitions = 40 (48), and total acquisition time = 78s (94s).

3.2 Pre-Processing

Motion-correction is carried out to establish a valid inter-pixel correspondence over time. It is essential when breathing, heartbeat, patient movement, or muscle relaxation occur. A visual inspection of all four datasets showed that the second scan $PS_{fup(2)}$ of the follow-up study suffered from a severe motion artifact during the first pass of CA. Hence, it was motion corrected in *MeVisLab* (www.mevislab.de), a platform for medical image processing and visualization, applying the algorithm developed by Rueckert et al. [13]. This algorithm combines rigid and elastic registration based on normalized mutual information and a gradient descent method for optimization. In a next step, all scans of PS_{fup} were registered to the first scan $PS_{fup(1)}$ using the software *RView* (rview.colin-studholme.net) which employs a rigid registration algorithm [17]. The registration supports a concurrent analysis of all three scans. Next, the brain was separated from the background in all datasets by means of a statistically derived intensity threshold. Finally, the signal intensities in all datasets were converted to changes in CA concentration according to [12].

3.3 Four Interactive Approaches to Investigating Cerebral Perfusion

Compared to an algorithmic analysis of perfusion data, our interactive analysis approaches require the user to eventually decide which part of the tissue is ranked among infarcted and healthy tissue, respectively. Hence, a ranking strategy needs to be specified. To distinguish infarcted tissue, a selection was initialized and then, extended by the user as long as the newly incorporated voxels were located only in the hemisphere affected by the stroke. This simple strategy is valid for investigating unilateral infarctions. In selecting infarcted tissue, no difference was made between the infarction core and the surrounding penumbra.

3.3.1 The Visual Analysis Framework

Our visual analysis concept is implemented in a framework employing the *SimVis* (www.simvis.at) technology [3]. In *SimVis*, multiple linked views are used to concurrently show, explore, and analyze different aspects of multi-field data. 3D views of the volume (also over time) can be used next to several types of attribute views, e.g., parallel coordinates, scatterplots or histograms. Interactive feature definition is usually performed in these attribute views (see Fig. 1 for an example). A more detailed review of the visual analysis framework can be found in [3].

3.3.2 Applying Concentration-time Curves

Muigg et al. [8] added a special attribute view to SimVis which facilitates a dense visualization of TICs or CTCs for all voxels of a perfusion data set (Fig. 1 (a)). Special techniques are used to reduce clutter in the visualization of a multitude of curves and dedicated brushes are employed to define curve target shapes. Such target shapes allow for an exploitation of expert knowledge since, e.g., clinicians are trained to infer tissue characteristics from curve shape. Besides the target shape, a similarity measure is applied to match the original curves with this shape.

The infarction core and the penumbra require the definition of two target shapes, one describing (almost) no enhancement and one describing a delayed and diminished enhancement during the CA's first pass. These shapes may to some degree be approximated by combining multiple vertical data interval brushes (*timestep brushes*) at different timesteps. However, a faster and more intuitive approach is the outlining of a target shape and the subsequent evaluation of the similarity measure. Two variants are implemented in SimVis. *Average Distance Brushes* employ the average distance between the target shape and the original curves as a similarity measure. *Gradient Sum Brushes* are based on the first derivatives of the target shape and the original curves. They employ the curve slope as a similarity measure and are hence, invariant to vertical translations. This property is especially attractive for the analysis of MR perfusion data since no standardized CA concentration values exist. The vertical extension of the brush defines the range of accepted values for the respective similarity measure.

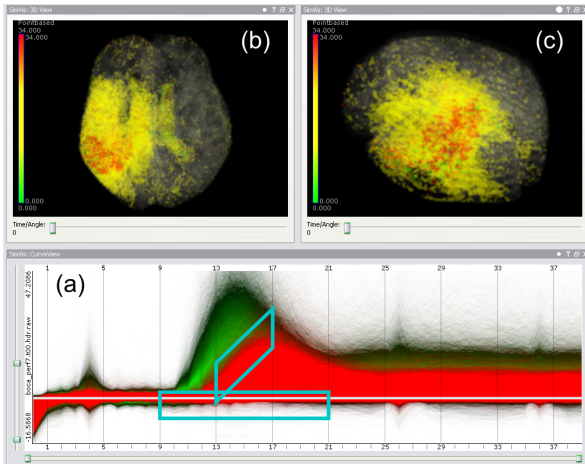


Figure 1. (a) The CTCs of the entire dataset *PS* are visualized. Two gradient sum brushes (turquoise boxes) have been defined. The selected curves are emphasized in red. (b) The brushing reveals infarcted tissue in one hemisphere. The tissue is colored according to the time until the maximum CA concentration is attained. (c) Its overall extension is illustrated by means of a lateral view.

In Fig. 1 (a), gradient sum brushes are defined to detect the infarcted tissue in *PS*. The horizontal and the slanted brush characterize the enhancement in the core and the penumbra, respectively. Their position and horizontal extension have been set up with respect to the location of the first pass. Together with the vertical extension and the slope, they have been adjusted according to the strategy described in Sec. 3. The selection result is visualized in Fig. 1 (b) and colored according to the time until the maximum of CA concentration is achieved. The infarction core appears reddish surrounded by the yellowish penumbra. The ventricles are also included in the selection since, similar to the core, no CA is accumulated here. A lateral view of the brain in Fig. 1 (c) shows the extension of the infarction zone over all slices. Such 3D views were highly appreciated by our clinical partners. Throughout the paper, the shape of the brain is indicated as context information in all 3D views. This is achieved by brushing the gradient magnitude computed from the CA concentration at the first timestep. This brushing has no impact on the infarction zone selection but also effects the coloring (slight green) of the attribute views.

Since the ventricles are not part of the infarcted tissue, they should be excluded from the selection. A subtracting timestep brush is defined on the first timestep such that large negative CA concentrations are excluded (see Fig. 2). These values roughly represent the ventricles and major arteries after conversion from signal intensity to CA concentration (see Fig. 8(ts1)). This is founded by the conversion formula [12] and the slightly higher signal intensities of the first timestep as compared to the rest. The latter originate from a pending steady-state condition for the MR signal.

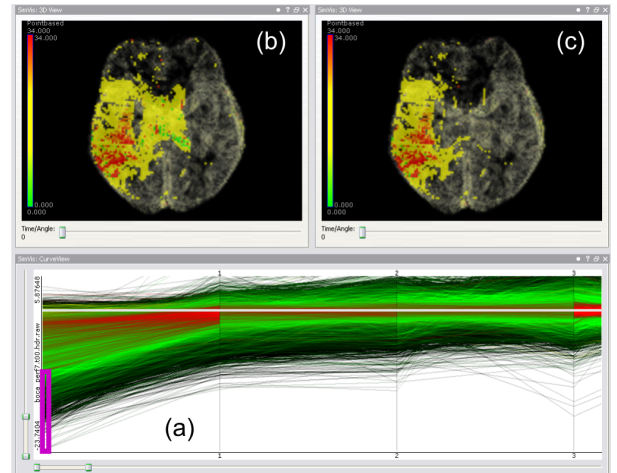


Figure 2. (a) The selection from Fig. 1(a) is refined such that the ventricles are excluded. This is illustrated in (b) and (c) only for a single slice to improve readability. In (a), the CTC visualization is zoomed in on the first four timesteps. The bright horizontal line represents the zero axis. A subtraction timestep brush (purple box) is defined such that large negative values are excluded.

3.3.3 Applying Descriptive Curve Shape Parameters

In cerebral perfusion diagnosis, parameters describing the curve shape during the first pass are derived region- or voxel-wise. In the following, we consider a voxel-wise analysis. A typical CTC with a significant first pass and an alleviated second pass of CA traversal annotated with the essential parameters is shown in Fig. 3. See [11] for a detailed description of all parameters as well as the auxiliary variables $Base_{Start}$, $CA_{arrival}$, $Time_{End}$, and $Baseline$. The latter are used for restricting the evaluation to the CA's first pass and to normalize the parameter values. We refer to the parameters which are derived directly from the CTCs as *descriptive parameters*. They do not facilitate a quantitative perfusion analysis which would require a determination of the arterial input function (see Sec. 3.3.5). The descriptive parameters have been computed in *MeVisLab*.

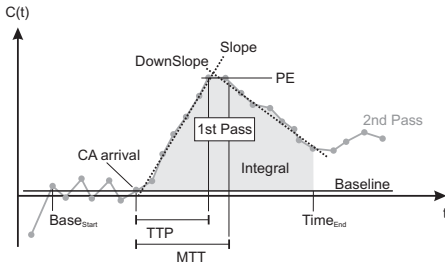


Figure 3. A typical CTC in cerebral perfusion annotated with the descriptive parameters.

For illustrating the feasibility of a concurrent analysis, the separate scans of PS_{fup} were integrated in a single dataset (Fig. 4 and Fig. 6). However, for the comparison of the visual analysis approaches in Sec. 4, each scan was treated separately. In Fig. 4, a parallel coordinates plot is employed to oppose all descriptive curve shape parameters. Each vertical line represents an axis of the 7-dimensional parameter space. Each voxel containing brain tissue is represented by a polyline whose vertices are constructed on these axes based on the respective parameter value. To generate a selection, vertical data interval brushes can be defined on each axis. In Fig. 4, first a brush was defined on TTP such that high values were selected. Next, a subtracting brush was defined on MTT to exclude outliers with a high TTP but a small MTT . The selection result is visualized in the 3D view and colored according to TTP . The view shows the three scans of PS_{fup} sorted by scanning order. The infarction core appears reddish in (1) and (2) and yellowish in (3). The concurrent analysis indicates that the penumbra benefited from the thrombolytic therapy.

3.3.4 Applying Enhancement Trends

Our previous work in [9] indicated a strong information redundancy in the higher dimensional space of descriptive parameters. This redundancy was resolved by a combination of correlation and Principal Component Analysis (PCA).

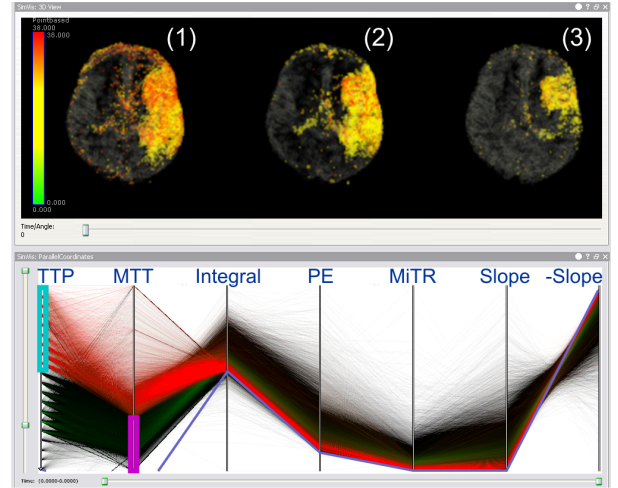


Figure 4. The parallel coordinates plot contains an axis for each descriptive parameter. A brush is defined on TTP such that high values are selected. A subtracting brush is then defined on MTT to exclude outliers with a small MTT . The 3D view shows the follow-up study sorted by scanning order. The selected tissue is colored according to TTP .

The latter revealed strong enhancement trends described by the first (pc_1) and second principal component (pc_2). These two trends were successfully applied in [9] for the detection of infarcted tissue in one example from cerebral perfusion (corresponding to PS). Hence, it was investigated here whether these trends may also be observed in the scans of PS_{fup} . For that purpose, a correlation analysis based on all descriptive parameters was carried out followed by an exclusion of highly correlated parameters. Then, a PCA was computed based on the reduced parameter set. See [9] for a more detailed description of the statistical analysis.

As can be inferred from Fig. 5, the first two pcs, i.e., the two strongest enhancement trends, are quite consistent across all datasets. Each bar of the plot represents a parameter *loading*, i.e., a weight for the linear combination of the n original variables. The prominent loadings are *Integral*

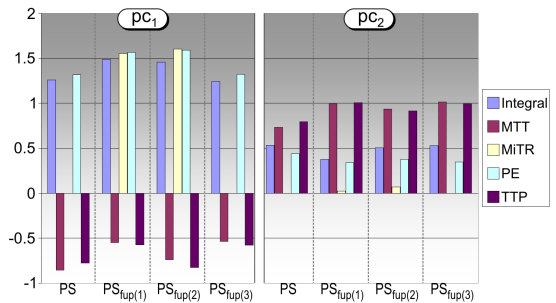


Figure 5. Perfusion parameter loadings of the first and second principal component (pc).

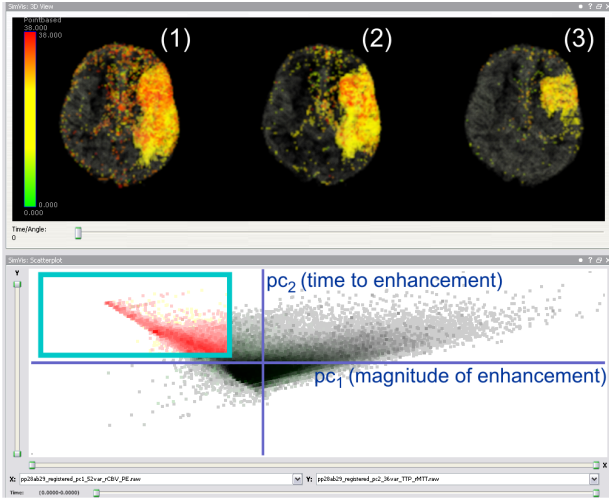


Figure 6. The scatterplot opposes the scores of the first and the second principal component. A brush encloses an area of low magnitude and long time. The 3D view shows the follow-up study sorted by scanning order. The selection is colored according to TTP . It well resembles the one obtained in Fig. 4.

and PE for pc_1 and MTT and TTP for pc_2 . $MiTR$ is only included for $PS_{fup(1-2)}$. For the remaining datasets, it was excluded before PCA due to its high correlations with other parameters. $Slope$ and $DownSlope$ were excluded for the same reason. On average, both pcs together account for $\approx 87\%$ of the variance in the data.

In order to employ the enhancement trends for a feature definition, their respective *scores* are opposed in a scatterplot (see Fig. 6). The scores are the coordinates of the original parameter space transformed into pc -space by a maximum variance rotation. The density of data values in the plot is opacity-coded. A meaningful label for the x-axis could be *Magnitude of Enhancement* with regard to pc_1 's prominent loadings. Accordingly, the y-axis could be labelled *Time to Enhancement*. A simple rectangular brush is defined enclosing an area with a low magnitude and a long time. The 3D view shows the three scans of PS_{fup} sorted by scanning order. The selection is colored according to TTP . It well resembles the one obtained in Fig. 4.

3.3.5 Applying Semi-quantitative Parameters

In order to obtain quantitative perfusion parameters, the arterial input function (AIF) must be determined. Then, the descriptive parameters must be normalized to the corresponding parameters of the AIF. Furthermore, the CTCs must be deconvolved with the AIF to obtain the cerebral blood flow [10]. However, even after normalization and deconvolution, parameter values are not yet in absolute physical units and only relative to their quantitative counterpart. A scaling is still necessary by a factor that depends on CA relaxivity, vascular structure, tissue density and hematocrit.

We omit this step since it is not crucial for our comparison of visual analysis approaches. We refer to the parameters without scaling as *semi-quantitative parameters*. The following semi-quantitative parameters are considered as essential in assessing stroke [16], [20] (recall Fig. 3):

- *relative Cerebral Blood Volume (rCBV)*: area under the CTC normalized to the area under the AIF,
- *relative Cerebral Blood Flow (rCBF)*: result of deconvolving the CTC with the AIF,
- *relative Mean Transit Time (rMTT)*: $\frac{rCBV}{rCBF}$,
- *Time To Peak (TTP)*

Optionally, a gamma variate function can be fitted to each CTC and the AIF before parameter computation. This step is referred to as *parametric modelling*. The fitting compensates for noisy data and reduces the effect of recirculation (recall Fig. 3). However, it may fail in areas with no distinctive CTC shape, i.e., abnormal hemodynamical conditions. For the comparison in Sec. 4, analysis results achieved with and without a fitting have been investigated.

The software *NordicICE* (www.nordicneurolab.com) was employed for computing the semi-quantitative parameters. Here, the widespread standard regularized Singular Value Decomposition [10] was chosen for deconvolution. The AIF was computed automatically for a user-defined subregion which was chosen such that severely diseased vessels were not included. The parameters computed by *NordicICE* are $rCBV$, $rCBF$, $rMTT$, and TTP . The selection of infarcted tissue in this four-dimensional parameter space was carried out as described in Sec. 3.3.3.

In Fig. 7 (left), a selection based on semi-quantitative parameters whose computation involved both, fitting and deconvolution is presented. Compared to Fig. 1(b), a considerable amount of small disconnected regions exists besides the infarction zone. In Fig. 7 (middle), the selection was reduced to voxels where the fitting had failed. *NordicICE* assigned a unique value to all parameters for these voxels. The largest connected component represents the infarction core and parts of the ventricles. However, small disconnected regions indicate the existence of more tissue with no distinctive CTC shape. A comparison with the selection based on parameters whose computation involved no fitting (Fig. 7 (right)) supports this assumption.

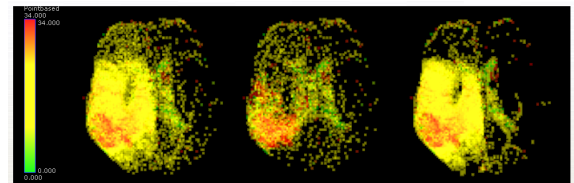


Figure 7. *Left*: selection based on semi-quantitative parameters whose computation involved fitting and deconvolution. *Middle*: selection reduced to voxels with a failed fitting. *Right*: selection achieved without a fitting.

4 Comparison

This section compares the four interactive approaches for feature definition and their variants presented in Sec. 3. To improve readability, we introduce abbreviations for the approaches based on: CTCs, with ($ACTC_{VR}$) and without ($ACTC$) a removal of the ventricles, descriptive curve shape parameters (ADP), enhancement trends (AET), and semi-quantitative parameters, with (ASQP) and without ($ASQP_{NoG}$) a preceding gamma variate fitting. The approaches differ concerning:

- the data, on which the feature definition is based (CTCs, descriptive curve shape parameters, pcs, semi-quantitative parameters),
- the kind of attribute view used for feature definition (curve view, parallel coordinate view, scatterplot), and
- the kind of applied brush (complex similarity brushes, 1D data interval brushes, 2D rectangular brushes).

Each approach was assessed with regard to the complexity of pre-processing necessary to generate the data on which the feature definition is based, and the complexity of the definition process itself.

The conversion of signal intensities to CA concentration [12] is demanded by all approaches. The applied formula requires the determination of $Base_{start}$ and $CA_{arrival}$ (recall Fig. 3) which can easily be accomplished by a visual inspection of the averaged TIC of the entire brain tissue. No additional pre-processing is required for $ACTC$ and $ACTC_{VR}$. ADP further demands a determination of the end of the CA's first pass ($Time_{End}$). In addition, a computation of the descriptive parameters is necessary which however, can be accomplished by simple mathematics. AET does also require the computation of the descriptive parameters. Moreover, a statistical analysis of these parameters is carried out, involving a correlation analysis, an exclusion of highly correlated parameters and a PCA. However, each step can be realized as a fully automatic process. ASQP and $ASQP_{NoG}$ both demand an AIF determination, a parameter computation and normalization, a deconvolution step and optionally, a fitting with a gamma-variate function (ASQP). While the remaining steps can be automatized, special care should be taken in AIF determination, i.e. selecting a candidate region which does not include severely damaged vessels. Overall, $ACTC$ and $ACTC_{VR}$ pose the least demands on pre-processing while AET, $ASQP_{NoG}$ and ASQP pose the highest demands. However, most of the necessary pre-processing can be carried out automatically.

The complexity of the feature definition process depends on the applied attribute view and the associated brushes. The gradient sum brushes used for $ACTC$ and $ACTC_{VR}$ are easy to set up. However, their fine-tuning requires some experience since not only CTCs having a gradient equal to the one of the brush are selected but a range of gradients as defined by the vertical extension of the brush. Furthermore, not only CTCs which pass through the brush but also vertically shifted CTCs with the wanted gradient properties

are selected. Although, this is a desired behavior, it still poses a discrepancy between the user expectations raised by the brush location and the selection result. Still, the gradient sum brushes provide the most intuitive way of integrating knowledge about curve shape into the feature definition. The parallel coordinates plot used for ADP, $ASQP_{NoG}$ and ASQP provides very simple 1D data interval brushes for each coordinate axis. However, the brushing may theoretically be carried out on seven or four axes. Our practical experiences indicated yet, that one brush defined on the TTP axis delivers a good initial result which may be refined by one or two additional (subtractive) brushes on other axes. The scatterplot used for AET facilitates the definition of a 2D rectangular brush. For all datasets, this feature definition process proved to be the quickest one in yielding satisfactory selections.

The evaluation of all analysis approaches also included an investigation of their individual selection results. These were examined with respect to:

- accuracy (overlap with the “real” infarction zone),
- compactness (existence of small, disconnected regions besides the infarction zone), and
- spurious inclusion of the ventricles.

Furthermore, all selections based on the same dataset were compared regarding their pair-wise and overall overlap and the averaged CTCs of their corresponding tissue.

To assess the accuracy of a selection, it was overlaid on the original 4D perfusion scan or the converted CA concentration data and inspected visually slice by slice in cine-mode (Fig. 8). In order to generate the overlay, isocontours were computed based on a binary mask image exported from *SimVis*. The visual inspection indicated no obvious over- or under-segmentation with neither of the feature definition approaches. However, it seemed that the selections based on ASQP contain the highest number of small disconnected regions besides the infarction zone (recall Fig. 7).

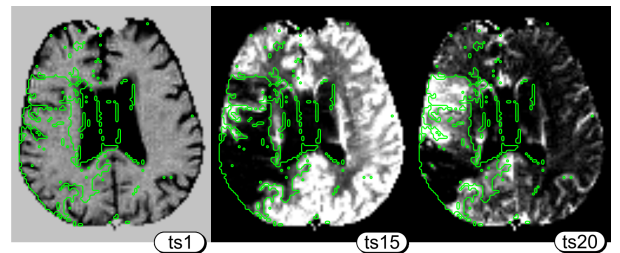


Figure 8. Slice of the dataset PS at three different timesteps with an overlaid selection result. The CA accumulation in healthy tissue is visible at an earlier timestep (ts15) as compared to the penumbral tissue (ts20).

For further investigation, the compactness of each selection was determined. First, its largest connected component (LCC) was computed considering a 6-connected neighborhood. For all selections, this resulted in a separation of

the infarction zone. Next, the percentage of voxels which are part of the entire selection (ES) but not part of LCC was computed. The higher the percentage, the smaller the compactness. A peak percentage (26.8%, averaged over all datasets) could be observed for the selections based on ASQP. The range of percentages for the remaining approaches was 12.2%-14.7%. The considerable difference as compared to the peak percentage confirms the observation of ASQP being the approach resulting in the highest number of small disconnected regions.

As described in Sec. 3, the ventricles may be spuriously included in the selection (recall Fig. 2). With non of the parameter-based approaches, it was possible to exclude the ventricles. Only the CTC-based analysis offered an opportunity by means of an additional subtractive timestep brush. This suggests that a parameter-based analysis may benefit from the integration of the original time-dependent information. Another beneficial application which cannot be described here in detail due to space restrictions is the handling of atypical CTC shapes caused by motion artifacts.

An interesting question is to what extent the different selections based on the same dataset overlap. A simple measure for this is the *Dice Coefficient (DC)* [19]. The values of DC are in the range from 0 (no overlap) to 1 (identical selections). We computed the pair-wise overlap for all selections as well as their overall overlap (see Fig. 9). The analysis shows the smallest pair-wise overlap ($\phi=0.69$) for all pairs including ASQP. The highest values ($\phi=0.93$) occur for the pair ACTC and ACTC_{VR} which can be expected since ACTC_{VR} is fully contained in ACTC. The remaining pair-wise overlaps are 0.79 on average.

The overall overlap is 0.53 on average (0.55 when discarding ACTC_{VR}). Only discarding ASQP from the computation leads to a considerable increase of DC ($\phi=0.16$ compared to $\phi=0.06$ for the remaining approaches). This is due to the high number of small disconnected regions generated by ASQP. Evaluating the overall overlap showed that besides a good-pair wise match, there still seem to be deviations across the selections. A visual inspection based on images such as Fig. 9 indicates that a lot of these deviations occur outside the infarction zone. The respective voxels each seem to be contained only in a small subset (< 3) of selections. By contrast, the majority of tissue that is part of all selections belongs to the infarction zone. However, these aspects should be confirmed by a more quantitative analysis. It should also be investigated to what extent the deviations are related to the fact that the feature definition is interactive and hence user-dependent.

Another interesting aspect in examining the parameter-based selections is the investigation of their counterpart in the original time-dependent perfusion data space. For that purpose, the averaged CTC was computed for each selection together with its standard deviation at each timestep. In Fig. 10, an error bar plot computed for dataset *PS* shows the averaged CTCs of all selections together with their standard deviations. The plot is superimposed on the filled reference curve computed from the healthy brain hemisphere. A high

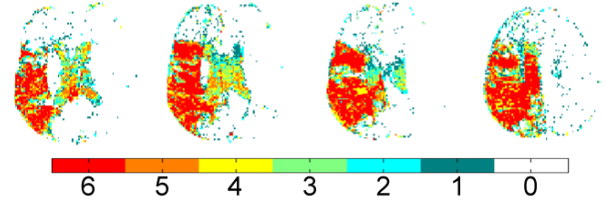


Figure 9. Visualization of the overall overlap of six selections based on the dataset *PS*. The color encodes the number of overlapping selections for a subset of four slices.

consistency of all selections can be inferred from the averaged CTCs. While their corresponding *Integral/rCBV* slightly varies, their *PE* is always located at timestep 18 which results in a consistent *TTP*. The delay with regard to the *TTP* of the reference curve (timestep 15) is 6 seconds ($(18-15) \times 2000\text{ms (TR)}$) which is in the range of typical values for penumbral tissue. Further evidence provide the smaller *Integral/rCBV* and *PE* values which indicate diminished perfusion.

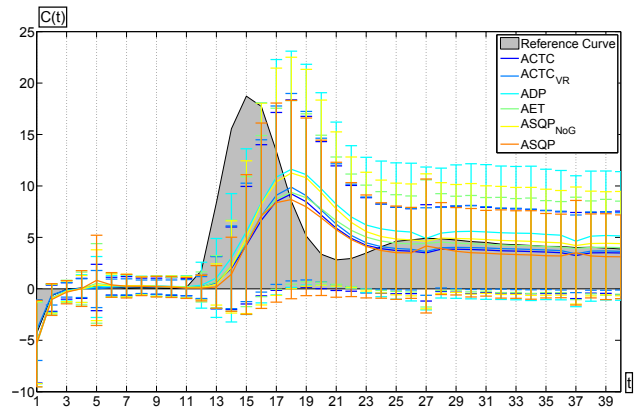


Figure 10. Error bar plot of the averaged CTCs corresponding to six selections based on the same dataset. The error bars represent the standard deviation of CA concentration per timestep. The reference curve has been derived from the healthy hemisphere.

5 Conclusion

We have presented and compared four interactive approaches to analyzing cerebral perfusion data from ischemic stroke patients which are based on (1) CTCs, (2) parameters describing the CTC shape, (3) enhancement trends computed in a statistical analysis, and (4) semi-quantitative perfusion parameters derived via parametric modelling and deconvolution with an arterial input function. The necessary pre-processing before an analysis can be carried out varies considerably between (1) and, e.g., (3) or (4). However,

most of the involved steps can be automatized. The feature definition process can be intuitively accomplished in (1) by means of CTC target shapes and a similarity measure. However, it is more complex compared to, e.g., (3) where only a rectangular brush has to be defined in 2D space. For all datasets, (3) proved to be the quickest approach in yielding satisfactory results. It needs further investigation whether this is due to the simple way of defining the brush or the easily possible differentiation of the infarction zone in the plot or both. An advantage of (1) is the ability to remove spuriously included ventricles from the selection based on the original time-dependent information. Furthermore, atypical CTC shapes caused by motion artifacts can be handled.

To assess the accuracy of all approaches in detecting infarcted tissue, the selection results were superimposed on the original data. A visual inspection indicated no obvious over- or under-segmentation with neither of the approaches. However, selections from (4), computed with a preceding gamma variate fitting, contained a high number of small disconnected regions besides the infarction zone. This could be traced back to a failure of the fitting in these regions due to the lack of a distinctive curve shape. It should be further investigated if this lack is due to local image noise or to compromised tissue perfusion with no or very little CA enhancement. The selections based on (1)-(3) and (4) without fitting, showed a considerable pair-wise overlap for the same dataset ($\phi=0.79$). A voxel ranking with respect to the number of containing selections showed that the majority of tissue that is part of all selections belongs to the infarction zone. Most of the small disconnected tissue regions are contained only in a small subset of selections. For the comparison of all selections based on the same dataset, the corresponding averaged CTCs were superimposed on a reference CTC derived from healthy tissue. A high consistency of all selections could be inferred from this superimposition. The described perfusion deficit and delay indicated a successful inclusion of the penumbra. Compared to an algorithmic analysis, an inherent property of our interactive approach is an inter- and intra-user variability of some degree. Their impact should be examined for a larger collection of data. In addition, the possibility of differentiating between infarction core and penumbra should be further investigated.

References

- [1] J. Blaas, C. Botha, and F. Post, "Interactive Visualization of Multi-field Data Using Dynamically Linked Physical and Feature Space Views", In *Proc. of EuroVis*, pp. 123–130, 2007.
- [2] E. Coto, S. Grimm, S. Bruckner, E. Gröller, A. Kanitsar, and O. Rodriguez, "MammoExplorer: An Advanced CAD Application for Breast DCE-MRI", In *Proc. of Vision, Modeling, and Visualization*, pp. 91–98, 2005.
- [3] H. Doleisch, M. Gasser, and H. Hauser, "Interactive Feature Specification for Focus+Context Visualization of Complex Simulation Data", In *Proc. of IEEE TCVG - EUROGRAPHICS Symp. on Vis.*, pp. 239–248, 2003.
- [4] Y.-H. Kao, M. M.-H. Teng, K.-C. Liu, I.-P. Lam, and Y.-C. Lin, "Hemodynamic Segmentation of MR Perfusion Images in Patients with Unilateral Carotid Stenosis Using Independent Component Analysis", *J Magn Reson Imaging*, 28(5), 2008, pp. 1125–32.
- [5] D. Lloyd-Jones, R. Adams, and M. Carnethon et al., "Heart Disease and Stroke Statistics–2009 Update", *Circulation*, 119(3), 2009, pp. e21–181.
- [6] A. Meyer-Baese, O. Lange, A. Wismueller, and M. K. Hurdal, "Analysis of Dynamic Susceptibility Contrast MRI Time Series Based on Unsupervised Clustering Methods", *IEEE Trans Inf Technol Biomed*, 11(5), 2007, pp. 563–73.
- [7] M. Mlejnek, P. Ermes, A. Vilanova, R. van der Rijt, H. van den Bosch, E. Gröller, and F. Gerritsen, "Application-Oriented Extensions of Profile Flags", In *Proc. of EuroVis*, pp. 339–346, 2006.
- [8] P. Muigg, J. Kehrer, S. Oeltze, H. Piringer, H. Doleisch, B. Preim, and H. Hauser, "A Four-level Focus+Context Approach to Interactive Visual Analysis of Temporal Features in Large Scientific Data", *Computer Graphics Forum (Proc. of EuroVis)*, 27(3), 2008, pp. 775–782.
- [9] S. Oeltze, H. Doleisch, H. Hauser, P. Muigg, and B. Preim, "Interactive Visual Analysis of Perfusion Data", *IEEE Trans. Vis. Comput. Graph.*, 13(6), 2007, pp. 1392–1399.
- [10] L. Ostergaard, R. M. Weisskoff, D. A. Chesler, C. Gyldensted, and B. R. Rosen, "High Resolution Measurement of Cerebral Blood Flow Using Intravascular Tracer Bolus Passages. Part I: Mathematical Approach and Statistical Analysis", *Magn Reson Med*, 36(5), 1996, pp. 715–25.
- [11] B. Preim, S. Oeltze, M. Mlejnek, E. Gröller, A. Hennemuth, and S. Behrens, "Survey of the Visual Exploration and Analysis of Perfusion Data", *IEEE Trans. Visual. Comp. Graphics*, 15(2), 2009, pp. 205–220.
- [12] B. R. Rosen, J. W. Belliveau, J. M. Vevea, and T. J. Brady, "Perfusion Imaging with NMR Contrast Agents", *Magn Reson Med*, 14(2), 1990, pp. 249–65.
- [13] D. Rueckert, L. Sonoda, C. Hayes, D. Hill, M. Leach, and D. Hawkes, "Nonrigid Registration Using Free-Form Deformations: Application to Breast MR Images", *IEEE Trans. Med. Imaging*, 18(8), 1999, pp. 712–721.
- [14] P. Schellinger, J. B. Fiebach, and O. Jansen et al., "Stroke Magnetic Resonance Imaging Within 6 Hours After Onset of Hyperacute Cerebral Ischemia", *Ann Neurol*, 49(4), 2001, pp. 460–9.
- [15] A. Sorensen, F. Buonanno, and R. Gonzalez et al., "Hyperacute Stroke: Evaluation With Combined Multisection Diffusion-weighted and Hemodynamically Weighted Echoplanar MR Imaging", *Radiology*, 199(2), 1996, pp. 391–401.
- [16] A. Sorensen, W. Copen, and L. Ostergaard et al., "Hyperacute Stroke: Simultaneous Measurement of Relative Cerebral Blood Volume, Relative Cerebral Blood Flow, and Mean Tissue Transit Time", *Radiology*, 210(2), 1999, pp. 519–527.
- [17] C. Studholme, D. L. G. Hill, and D. J. Hawkes, "An Overlap Invariant Entropy Measure of 3D Medical Image Alignment", *Pattern Recognition*, 32(1), 1999, pp. 71 – 86.
- [18] M. Takasawa, P. S. Jones, and J. V. Guadagno et al., "How Reliable is Perfusion MR in Acute Stroke? Validation and Determination of the Penumbra Threshold Against Quantitative PET", *Stroke*, 39(3), 2008, pp. 870–7.
- [19] C. v. Rijsbergen, *Information Retrieval*, Butterworth, 1979.
- [20] H.-J. Wittsack, A. Ritzl, and G. R. Fink et al., "MR Imaging in Acute Stroke: Diffusion-weighted and Perfusion Imaging Parameters for Predicting Infarct Size", *Radiology*, 222(2), 2002, pp. 397–403.